Direct observation of partial disorder and zipperlike transition in crystalline phase change materials

Min Zhu,[1,*] Kun Ren,[1] Long Liu,[2] Shilong Lv,[1] Xiangshui Miao,[2] Ming Xu,[2,†] and Zhitang Song[1,‡]

[1]*State Key Laboratory of Functional Materials for Informatics, Shanghai Institute of Micro-System and Information Technology,*
Chinese Academy of Sciences, Shanghai 200050, China
[2]*Wuhan National Research Center for Optoelectronics, School of Optical and Electronic Information,*
Huazhong University of Science and Technology, Wuhan 430074, China

Chalcogenide phase change materials, such as $Ge_1Sb_2Te_4$ (GST), are of tremendous importance in emerging data storage technology, which takes advantage of rapid and reversible switching of GST between the amorphous and crystalline phases. To date, however, the atomic arrangement of the crystalline GST structure has not been fully resolved, resulting in a controversial understanding of the polymorphic transition mechanism. Here, the atomic and chemical arrangements of stable hexagonal structures of GST are determined by state-of-the-art aberration-corrected scanning transmission electron microscopy. A partially ordered Ge/Sb atomic stacking is resolved in the hexagonal structure to balance the enthalpy and entropy, differing from completely disordered Ge/Sb intermixing arrangement in a metastable rock-salt structure. The transition mechanism between these two phases is proposed, achieved by opening the van de Waals gap like a zipper triggered by the Ge/Sb hopping near vacancy grooves rather than the interplanar random atomic migration. The present results shed light on the understanding of the atomic arrangement and polymorphic phase transitions as well as the control of disorder in GST phase change memory.

Phase change materials (PCMs), primarily $GeTe$-Sb_2Te_3 pseudobinary alloys (GST), have been extensively exploited in optical/electrical data storage, flexible displays, and brain-inspired computing [1–3]. The application of memory devices is enabled by nanosecond phase transition of PCMs between the amorphous and crystalline phases with large property contrast [4,5]. Crystalline GST presents a metastable rock-salt (RS) phase and a stable trigonal or hexagonal (HEX) phase at ambient conditions [6,7]. The atomic arrangement of the latter is generally employed as a model system to understand the structural detail of $(GeTe)_x(Sb_2Te_3)_y$ superlattice memory (known as interfacial phase change memory, iPCM), which exhibits significantly faster speed and lower switching energy than the conventional alloy-based one [8,9]. Moreover, the structural transition between RS and HEX phases plays a vital role in shaping the transport properties of GST PCM for multiple-level storage [10,11]. However, due to the limits of characterization techniques, the structural model of the HEX phase and underlying transformation mechanism are still unclear.

The RS phase has been proved to have two sublattices, one made of only Te and the other one randomly occupied by Ge, Sb, and vacancy [12]. Generally, the HEX phase comprises repetitive seven-layered blocks, separated by van der Waals (vdW) gaps [6]. Three stacking models of the unit block have already been proposed [13–15], namely, Te-Ge-Te-Sb-Te-Sb-Te-Ge-Te (Petrov

model), Te-Sb-Te-Ge-Te-Ge-Te-Sb-Te (Kooi model), and Te-Ge/Sb-Te-Ge/Sb-Te-Ge/Sb-Te-Ge/Sb-TeTe-Ge/Sb-Te-Ge/Sb-Te-Ge/Sb-Te-Ge/Sb-Te (Matsunaga model; Ge/Sb denotes a mixed layer). Among these models, the Kooi model was found to be energetically favorable based on density functional theory (DFT) [16]. In contrast, through the hybrid functional calculations, a mixed-layer configuration was considered to be the most stable one [17]. Further progress has been made through high-angle angular dark field (HAADF) scanning transmission electron microscopy (STEM) that the Sb atoms in mixed Ge/Sb layers tended to aggregate in the planes near vdW gaps [18].

The vaguely determined HEX structure results in utterly different RS-to-HEX transformation mechanisms. Park *et al.* considered that the transformation could be achieved by exchanging the position of Ge and Sb atoms [19], whereas Sun *et al.* concluded that it was accomplished by the slipping of the -Te-Sb-Te-Ge- block in the RS phase along the [210] direction [16]. The DFT study carried out by Zhang *et al.* [11] described this transition as the diffusion of vacancies into certain layers, followed by the ordering of Ge/Sb layers. The formation of vacancy clusters was also believed to be responsible for the metal-insulator transition. Subsequent experiments confirmed the ordered vacancy layers in RS structure, realized by electron-beam irradiation [20].

A solid picture of the atomic arrangements of HEX phases is the prerequisite for understanding the structural detail of iPCM and the underlying RS-to-HEX transformation mechanism, which is the goal of this paper. In this work, we present the direct atom-resolved picture of HEX structures of $Ge_1Sb_2Te_4$ (GST), one of the best-performance prototypes, by state-of-the-art aberration-corrected STEM imaging. A

———————
*minzhu@mail.sim.ac.cn
†mxu@hust.edu.cn
‡ztsong@mail.sim.ac.cn

FIG. 1. Structural and chemical identifications in a $Ge_1Sb_2Te_4$ crystallite with HEX phase, projected along the [11-20] direction. (a) HAADF-STEM image of the transition region. The arrows mark the vdW gap between two blocks. (b)–(h) EDX mappings for Ge, Sb, Te, Ge/Sb, Ge/Te, Sb/Te, and Ge/Sb/Te elements, respectively.

$\sim$ 600-nm-thick GST film was deposited on Si substrate by physical vapor deposition using an alloy target. The film was cut into four pieces and annealed at 300 °C for 5, 30, 60, and 90 minutes, respectively, to get the structural evolution of GST film. Subsequently, four TEM lamella were prepared from these specimens using a focused ion beam. The atomic-resolution STEM experiments were performed on a JEM-ARM300F microscopy equipped with double probe Cs corrector, three detectors, and an energy-dispersive x-ray (EDX) spectroscope. The HAADF images were obtained at 80 or 300 kV, while EDX mappings were carried out at 80 kV. A probe forming aperture of 22.1 mrad was used in the experiments. A STEM image was performed using 50–200 mrad annular ranges of the HAADF detector, whereas 24–96 mrad annular ranges of the ADF detector were used for obtaining the ADF image.

For the sample annealed at 300 °C for 5 minutes, most of the film has crystallized into the HEX phase with visible vdW gaps, yet some areas are still in the RS phase due to inhomogeneous annealing (see Fig. S1 in the Supplemental Material [21]). The grain grows along the [11-20] direction, from which the cation planes (Ge and Sb) are not mixed with the anions (Te). The HAADF-STEM image clearly exhibits the presence of 7 and 9 stacking blocks in the [11-20]-oriented grain, belonging to GST and $Ge_2Sb_2Te_5$ stoichiometries, respectively, which has been previously reported by Mio *et al.* [18]. This is because the total energies of the three equilibrium phases in $GeTe$-Sb_2Te_3 pseudobinary alloys, namely, $Ge_1Sb_2Te_4$, $Ge_2Sb_2Te_5$, and $Ge_1Sb_4Te_7$ with respective 7-, 9-, and 12-plane stacking block, are not so different (–0.79, –0.97, and –1.38 eV, respectively) [22].

Nevertheless, most of the blocks are stacked with seven-layer atoms in HEX-GST, as present in Fig. 1(a), indicating that other types of stacking blocks are merely intermediate phases. The HAADF-STEM image presents a stacking sequence parallel to vdW gaps, with high/low/high/low/high/low/high intensity. Since the intensity (brightness of the image) is roughly proportional to $Z^{1.7}$ in the HAADF mode [23], where Z represents the average atomic number of atoms, the bright spots mean the occupancy of heavier atoms, i.e., Te atoms ($Z_{Ge} = 32$, $Z_{Sb} = 51$, $Z_{Te} = 52$), whereas the dark ones should be Ge or Sb or a mixture of them, which can hardly be distinguished from the Z contrast.

To distinguish Ge and Sb, advanced scanning EDX analysis was performed on the same area, and the results are shown in Figs. 1(b)–1(h). From the EDX mapping of individual Ge, Sb, and Te species in Figs. 1(b)–1(d), we can determine that Ge/Sb and Te atoms are in separated sublattices, without obvious antisite diffusion. Noticeably, the intensity of the centered Ge layer (Layer A) is apparently higher than the other two (Layer B) that are near the vdW gaps and, equivalently, Sb layers show an opposite trend. These phenomena can be observed more clearly from the combination of single constituent images, as presented in Figs. 1(e)–1(h), in which red, green, and blue atoms represent Ge, Sb, and Te, respectively. Apparently, Ge and Sb atoms are located at the same sublattices, as illustrated in Fig. 1(e). Unexpectedly, their distributions are definitely inhomogeneous since Layer A obviously has more Ge (redder) than Layer B (greener). In other word, Ge atoms preferentially lie at the center of the block, while Sb atoms incline to concentrate near the vdW gaps. By analyzing the EDX point scanning images, we
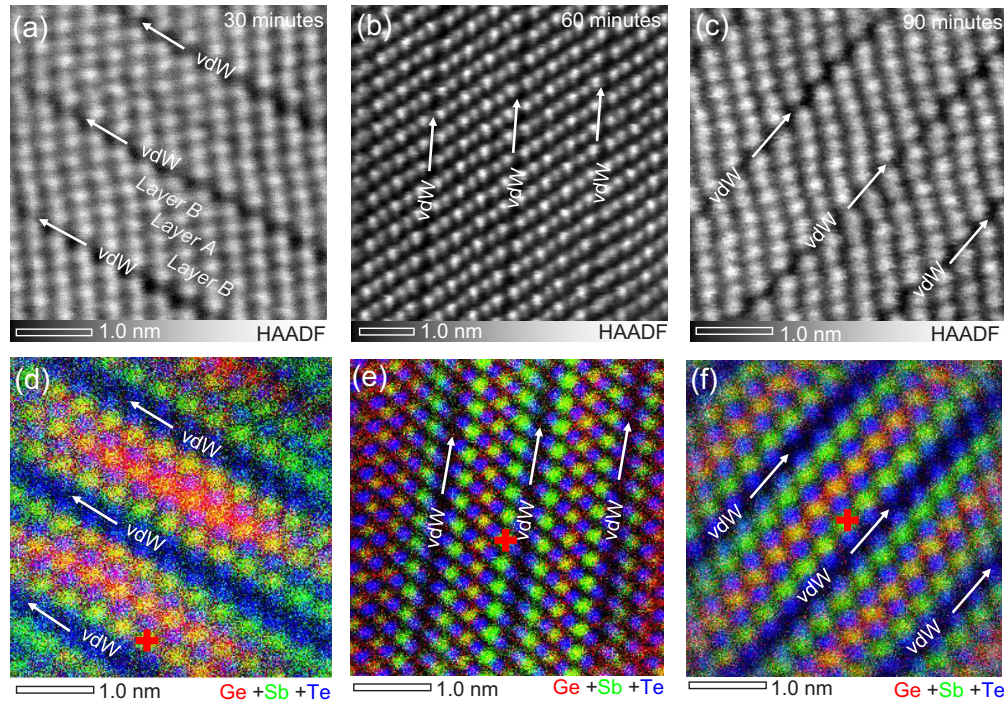
FIG. 2. The evolution of disorder for $Ge_1Sb_2Te_4$ annealed at 300 °C for different holding time. (a)–(c) HAADF-STEM images of seven-layer blocks annealed for 0.5, 1, and 1.5 hours. (d)–(f) Corresponding EDX mappings of overlaid Ge/Sb/Te elements. The red cross highlights the Ge/Sb atomic column for EDX point scan.

estimated that the Ge concentration in Layer B is estimated to ~ 20 at.% after rapid annealing, as shown in Table 1 in the Supplemental Material [21].

One may argue that the inhomogeneous distribution of Ge/Sb is probably due to the incomplete phase transition, while our long-time annealing process does not completely eliminate this "partial disorder" (Fig. 2). Since the specimen drifts too swiftly to get the atomic-resolution images of transitions in the *in situ* study, here four samples annealed at 300 °C for different durations were investigated instead. By extending the annealing time from 5 to 60 minutes, the concentration of Ge in Layer B reduces by only 3–4 at.% (Table 1 in the Supplemental Material [21]), which remain $\sim 16\%$ for longer time (90 minutes). This clearly suggests that the partially disordered arrangement with $\sim 16\%$ Ge concentration in Layer B is probably the stable configuration for HEX-GST. Similarly, the nine-layer blocks found in the HEX-GST, typical repeated units of $Ge_2Sb_2Te_5$, also present a partially ordered atomic arrangement (Fig. S2 in the Supplemental Material [21]). Hence, the data displayed here explicitly determine that the structural and chemical arrangement of the HEX phase in GST, as well as GeTe-Sb_2Te_3 pseudobinary alloys, is neither a completely disordered configuration (Matsunaga model) nor a completely ordered one (Kooi model). The Ge/Sb layers in the HEX phase tend to be stabilized at a specific degree of disorder, and a longer annealing time drives the system to approach such a configuration.

A question then arises: why does the HEX phase favor a certain degree of disorder? In traditional thermodynamics, this usually originates from the balance between enthalpy which favors the order of system and the entropy that entails disorder. We start from calculating the enthalpy of various HEX-GST

structures from a completely ordered Ge/Sb layer to a totally disordered one using the DFT method (computational details are listed in the Supplemental Material [21]) [24–26]. We use a "disorder parameter" p to quantitate the degrees of disorder in the Ge/Sb layers. p is defined by the percentage of Ge in Layer B (the Ge/Sb layers near vdW gaps), and thus $p = 0$ refers to a perfectly ordered HEX structure, while $p = 1/3$ represents the random mixture of Ge/Sb in HEX-GST. The following task is to find out which p value is the most favorable at room temperature.

Our DFT results as well as earlier reports [27] point out that the enthalpy (H) of the completely ordered configuration ($p = 0$) is the lowest, and H appears to monotonously increase with the disorder parameter p; see Fig. 3(a). Nevertheless, the enthalpy difference (ΔH) between the lowest structure (-3.73191 eV/atom when $p = 0$) and the highest one (-3.72635 eV/atom when $p = 1/3$) is merely 5.56 meV per atom, which agrees well with the results reported before [28]. This minor enthalpy difference can be easily compensated by the entropy (S), which drives the system into a more disordered state. We derived how S changes with p at room temperature (computational details are listed in the Supplemental Material [21]). By adding up the enthalpy and entropy contributions, we have eventually determined the minimum transition energy (ΔG) when $p = 0.15$ that leads to the equilibrated state. $p = 0.15$ corresponds to the GST configuration with 15% Ge atoms and 85% Sb located in Layer B near vdW gaps, and 70% Ge and 30% Sb atoms lay at Layer A in the center of the block, consistent with the results obtained from EDS point scanning ($p = \sim 16\%$). This partially disordered configuration well explains the inhomogeneous distribution of Ge/Sb in Figs. 1(h) and 2(f).
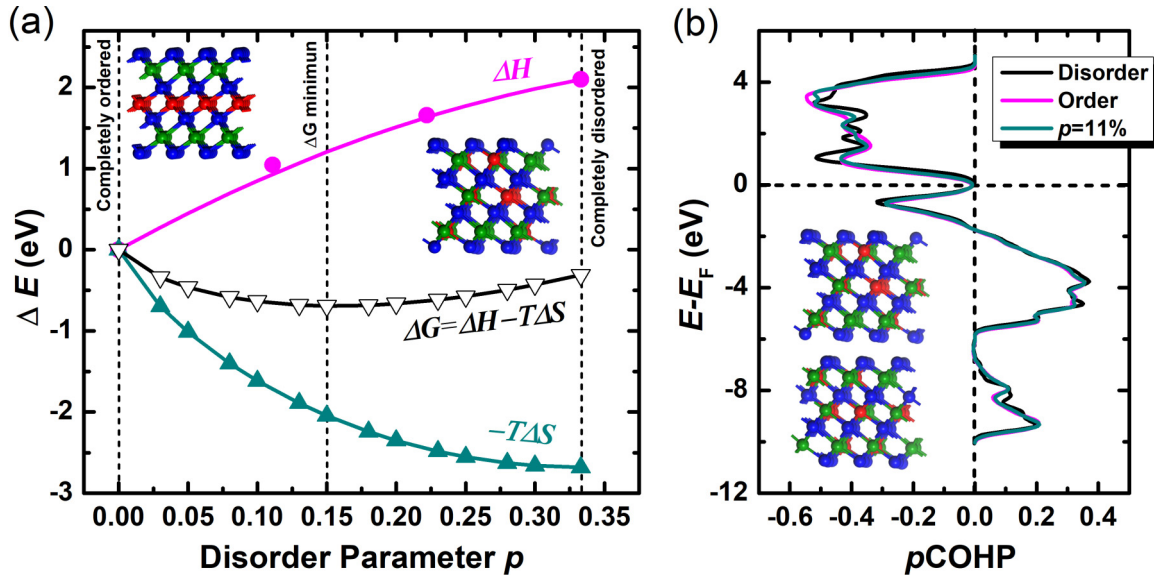
FIG. 3. (a) The enthalpy/entropy and the energy per cell (378 atoms) as a function of the disorder parameter p. The insets show the structure models for GST with $p = 0$ (left) and $p = 1/3$ (right), respectively. (b) The crystal orbital Hamilton population (COHP) analysis for HEX-GST with various degrees of order. Ge atoms: red; Sb atoms: green; Te atoms: blue. The inset shows the structure model for GST with $p = 11\%$.

The crystal orbital Hamilton population (COHP) bonding analysis in Fig. 3(b) further confirms that the partially ordered configuration is stable in terms of the bonding energy [29]. In this figure, pCOHP < 0 denotes the number of "antibonding states" which is detrimental to the formation of bonds and pCOHP > 0 represents the "bonding states" that favor the bonding. The COHP does not show a significant difference when we change the degrees of disorder, indicating that the disorder is not destructive to the cohesion of atoms. After all, the mixture of Ge/Sb layers does not lead to unfavorable homopolar bonds and the difference of enthalpy mainly stems from the secondary interaction. Moreover, the calculated lattice parameters from this model ($a = 4.293$ Å and $c = 40.479$ Å) match well with the experimental ones ($a = 4.21$ Å, $c = 40.6$ Å) [30]. Hence, we come to the conclusion that the partially ordered stacking structure with $p = 15\%$, that is, -Te-Ge$_{0.15}$Sb$_{0.85}$-Te-Ge$_{0.7}$Sb$_{0.3}$-Te-Ge$_{0.15}$Sb$_{0.85}$-Te-vdW-, determined by evaluating the interplay between the enthalpy and entropy, is regarded as the stable configuration of HEX-GST at room temperature. This interplay may also be responsible for the recently found strong Ge/Sb intermixing GeTe/Sb$_2$Te$_3$ superlattice [31], which completely reconfigures into an ordered GST structure (seven-layer or nine-layer) after high-temperature annealing [32].

Now that we have determined the stable HEX structures in GST, the next challenge is to uncover the mechanism of the phase transformation from RS to HEX on the atomic scale. As presented in Figs. 4(a) and 4(b), the RS structure has two clearly discernable sublattices: one sublattice occupied by Te only and the other one randomly occupied Ge, Sb, and vacancies. Unfortunately, the aberration-corrected STEM technique fails to resolve the positions of vacancies because they are randomly intermixed in the Ge/Sb sublattice (seen details in Fig. S3 in the Supplemental Material [21]). We found that the vacancy layers (VLs), which are quite common defects observed by STEM (Fig. S5(a) in the Supplemental

Material [21]), frequently appear in the intermediate areas between the RS and HEX phases [33,34]. Due to the low electron density, these VLs are characterized by one-fourth intensity [Fig. S4(b) in the Supplemental Material [21] and dark regions in Fig. 4(c)] compared to other atoms, and they recur regularly in every 7/9 atomic planes. This implies that about half of the Ge/Sb atoms are moved in these VLs. The spatial width of VLs is ~3.5 Å, almost equal to the interplanar spacing between two Te layers in the RS phase but ~1.0 Å wider than the vdW gap (~2.8 Å) in the HEX phase. The wide space of VLs indicates that they are the precursors (or unfinished products) of vdW gaps. As seen from the EDX mapping in Fig. 4(d), Sb signals are much weaker in VLs than other Ge/Sb planes, whereas those of the neighboring Ge/Sb planes are the strongest. In contrast, Te atoms are almost immobile (no large hopping) during the transition and they act as the structural frame of both RS and HEX GSTs (Fig. S4(d) in the Supplemental Material [21]). This leads to the postulation that Ge/Sb atoms in VLs move into vacancies in the nearby Ge/Sb layers, formatting an atomic arrangement that closely resembles the partially ordered HEX phase.

Figure 4(e) illustrates the most probable mechanism of the phase transition from RS to HEX. Initially, driven by thermal fluctuation, minor Ge/Sb atoms from every four Ge/Sb planes in RS-GST stochastically break three bonds, penetrating through the Te planes and "exchanging" sites with vacancies in the nearby Ge/Sb planes. Actually, the activation energy for such a random migration of Ge/Sb atoms is rather large, calculated to be around 0.8 and 1.0 eV/atom (Fig. 4(g); the computational method is described in the Supplemental Material [21]), respectively. However, as long as the flipping of Ge/Sb atoms takes place near VLs, the energy barrier is remarkably reduced to ~0.3 eV [Fig. 4(g)]. This is because the Te atoms near VL give way to the subsequent Ge/Sb flipping [indicated by the blue arrow in Fig. 4(f)]. Subsequently, Sb-rich Ge/Sb atomic arrangements would be achieved
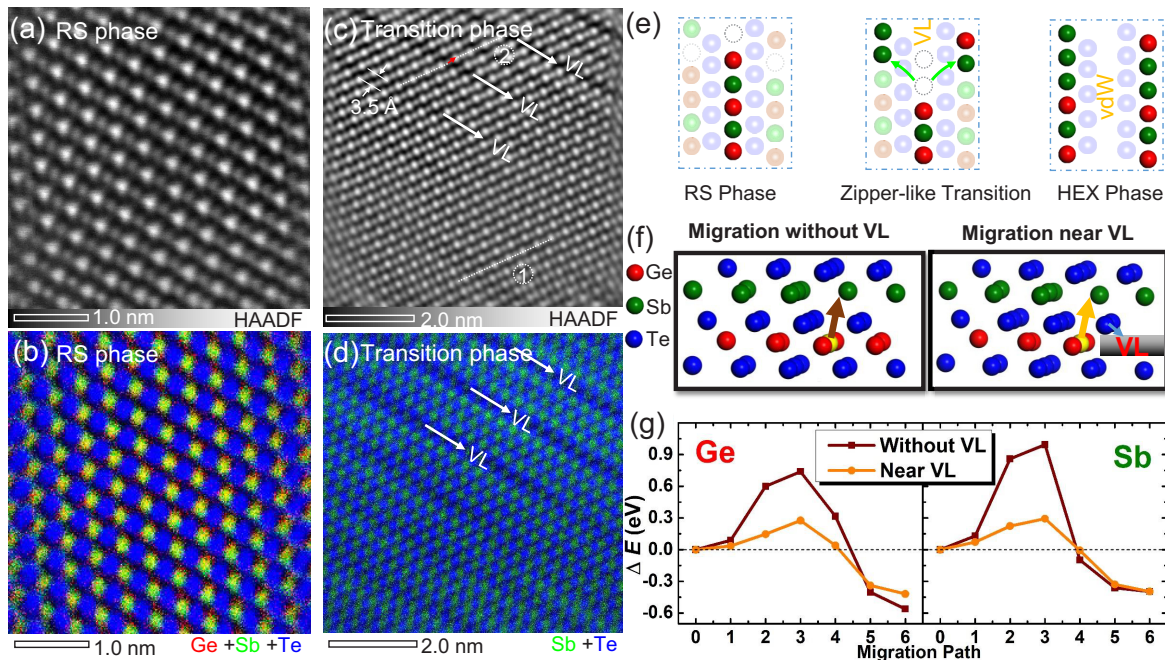
FIG. 4. Structural and chemical identifications of a $Ge_1Sb_2Te_4$ crystallite transiting from the RS phase to the HEX phase. (a), (b) HAADF-STEM image and EDX mapping of overlaid Ge/Sb/Te of rock-salt region. (c) HAADF-STEM image of the transition region. The region is projected along the [110] direction. The arrows mark the vacancy layers, the width of which is ~3.5 Å. The sliding of a seven-layer block, marked by the red arrow, is also observed comparing lines 1 and 2. (d) EDX mapping for overlaid Sb/Te. (e) The proposed model of the zipperlike transformation from RS to HEX. (f) The migration models of Ge/Sb atoms into vacant sites in the adjacent Ge/Sb planes with and without VL. (g) The calculated energy for Ge/Sb-vacancy jump processes with and without VL.

effortlessly through such zipperlike flipping processes. After repeated atomic hoppings, the intermediate phase undergoes a relaxation process, and vdW gaps are created by shortening of VLs as well as sliding of the blocks, as seen in line 2 in Fig. 4(c). Since the grain boundary has enormous vacancy defects, served as VLs, the transition would generally trigger from the grain boundary, just as seen in Fig. S4 in the Supplemental Material [21] and in Ref. [20]. Such an energy-effective zipperlike transition can explain the coexistence of both RS and HEX in the GST phase change memory cell after repeated cycle operations [35,36].

To summarize, atomic arrangements for HEX phases of GST PCM were determined by state-of-the-art aberration-corrected STEM technology. A partially ordered Ge/Sb atomic stacking manner is observed directly in the repeated blocks of the HEX phase separated by vdW gaps. Such a specific configuration stems from the interplay between the formation enthalpy and the entropy. The polymorphic transition between these two phases is achieved by the flipping of Ge/Sb atoms near the precursor VLs into vacant sites in adjacent Ge/Sb sublattices, and the vdW gaps in the HEX structure are opened in a zipperlike fashion. The atomic stacking sequence that closely resembles the partially ordered HEX structure is effortlessly obtained after this zipperlike transition instead of an energetically unfavorable random atomic migration. These findings provide clear pictures of the atomic arrangement of GST, solving a longstanding puzzle for this material.

[1] M. Wuttig and N. Yamada, Nat. Mater. **6**, 824 (2007).

[2] P. Hosseini, C. D. Wright, and H. Bhaskaran, Nature (London) **511**, 206 (2014).

[3] D. Kuzum, R. G. D. Jeyasingh, B. Lee, and H.-S. P. Wong, Nano Lett. **12**, 2179 (2012).

[4] M. Zhu, M. Xia, F. Rao, X. Li, L. Wu, X. Ji, S. Lv, Z. Song, S. Feng, H. Sun, and S. Zhang, Nat. Commun. **5**, 4086 (2014).

[5] M. Zhu. *Ti-Sb-Te Phase Change Materials: Component Optimisation, Mechanism and Application* (Springer, Singapore, 2017).

[6] N. Yamada, E. Ohno, K. Nishiuchi, and N. Akahira, J. Appl. Phys. **69**, 2849 (1991).

[7] M. Xu, Y. Q. Cheng, H. W. Sheng, and E. Ma, Phys. Rev. Lett. **103**, 195502 (2009).

[8] R. E. Simpson, P. Fons, A. V. Kolobov, T. Fukaya, M. Krbal, T. Yagi, and J. Tominaga, Nat. Nanotechnol. **6**, 501 (2011).

[9] J. Tominaga, A. V. Kolobov, P. Fons, T. Nakano, and S. Murakami, Adv. Mater. Inter. **1**, 1300027 (2014).

[10] T. Siegrist, P. Jost, H. Volker, M. Woda, P. Merkelbach, C. Schlockermann, and M. Wuttig, Nat. Mater. **10**, 202 (2011).

[11] W. Zhang, A. Thiess, P. Zalden, R. Zeller, P. H. Dederichs, J.-Y. Raty, M. Wuttig, S. Blugel, and R. Mazzarello, Nat. Mater. **11**, 952 (2012).

[12] T. Nonaka, G. Ohbayashi, Y. Toriumi, Y. Mori, and H. Hashimoto, Thin Solid Films **370**, 258 (2000).

[13] I. I. Petrov, R. M. Imamov, and Z. G. Pinsker, Sov. Phys. Crystallogr. **13**, 339 (1968).

[14] B. J. Kooi and T. T. M. De Hosson, J. Appl. Phys. **92**, 3584 (2002).

[15] T. Matsunaga, N. Yamada, and Y. Kubota, Acta Crystallogr. Sect. B **60**, 685 (2004).

[16] Z. Sun, J. Zhou, and R. Ahuja, Phys. Rev. Lett. **96**, 055507 (2006).

[17] G. C. Sosso, S. Caravati, C. Gatti, S. Assoni, and M. Bernasconi, J. Phys.: Condens. Matter **21**, 245401 (2009).

[18] A. M. Mio, S. M. S. Privitera, V. Bragaglia, F. Arciprete, C. Bongiorno, R. Calarco, and E. Rimini, Nanotechnology **28**, 065706 (2017).

[19] Y. J. Park, J. Y. Lee, M. S. Youm, Y. T. Kim, and H. S. Lee, J. Appl. Phys. **97**, 093506 (2005).

[20] A. Ltonyk, S. Bernutz, X. Sun, U. Ross, M. Ehrhardt, and B. Rauschenbach, Acta Mater. **105**, 1 (2016).

[21] See Supplemental Material at http://link.aps.org/supplemental/10.1103/PhysRevMaterials.3.033603 for a detailed description of the atomic arrangement and chemical identification of rocksalt and hexagonal GST, the transition area, as well as methods to calculate the enthalpy and energy barrier.

[22] V. L. Deringer and R. Dronskowski, J. Phys. Chem. C **117**, 15075 (2013).

[23] M. Küpers, P. M Konze, S. Maintz, S. Steinberg, A. M. Mio, O. C. Mirédin, M. Zhu, M. Müller, M. Luysberg, J. Mayer, M. Wuttig, and R. Dronskowki, Angew. Chem. Int. Ed. **56**, 10204 (2017).

[24] G. Kresse and J. Furthmuller, Comput. Mater. Sci. **6**, 15 (1996).

[25] P. E. Blochl, Phys. Rev. B **50**, 17953 (1994).

[26] Y. Wang and J. P. Perdew, Phys. Rev. B **44**, 13298 (1991).

[27] M. Xu, W. Zhang, R. Mazzarello, and M. Wuttig, Adv. Sci. **2**, 1500117 (2015).

[28] J. Singh, G. Singh, A. Kaura, and S. K. Tripathi, J. Solid State Chem. **260**, 124 (2018).

[29] S. Maintz, V. L. Deringer, A. L. Tchougreeff, and R. Dronskowski, J. Comput. Chem. **34**, 2557 (2013).

[30] T. Matsunaga and N. Yamada, Phys. Rev. B **69**, 104111 (2004).

[31] R. Wang, V. Bragaglia, J. E. Boschker, and R. Calarco, Cryst. Growth Des. **16**, 3596 (2016).

[32] J. Momand, R. Wang, J. E. Boschker, M. A. Verheijen, R. Calarco, and B. J. Kooi, Nanoscale **7**, 19136 (2015).

[33] U. Ross, A. Lotnyk, E. Thelander, and B. Rauschenbach, Appl. Phys. Lett. **104**, 121904 (2014).

[34] M. Behrens, A. Lotnyk, U. Ross, J. Griebel, P. Schumacher, J. W. Gerlach, and B. Rauschenbach, CrystEngComm **20**, 3688 (2018).

[35] Y. Wang, X. Chen, Y. Cheng, X. Zhou, S. Lv, Y. Chen, Y. Wang, M. Zhou, H. Chen, Y. Zhang, Z. Song, and G. Feng, IEEE Electr. Device Lett. **35**, 536 (2014).

[36] Y. T. Kim and Y. H. Kim, Phys. Status Solidi B **251**, 435 (2014).